OHID: A Large Hyperspectral Image Dataset for Classification

Jun Yan[1][0000−0003−2099−7162], Sergey Gorbachev[2][0000−0001−8096−1327], Xiaoxu Jiang[1*][0000−0002−8907−4481], Tengjie Huang[1][0000−0002−9376−6616], Jianwen Deng[1][0000−0002−6989−6824], and Xiaohua Jiang[1][0000−0002−4731−3827]

[1] Zhuhai Orbita Aerospace Science & Technology Co. Ltd, China;
yan@myorbita.net(J.Y.); jiangxx@myorbita.net(X.J.);
huangtj@myorbita.net(T.H.); dengjw@myorbita.net(J.D.);
jiang@myorbita.net(X.J.);
[2] Department of Innovative Technologies, National Research Tomsk State University, Tomsk, 634050 Russia;
hanuman1000@mail.ru(S.G.);
*Corresponding Author

Abstract. Hyperspectral images (HSI) have become an important data source for agricultural analysis, classification, and other remote sensing tasks. HSI classification is a significant task for HSI parsing. Currently, only about 20 hyperspectral satellites, including 8 hyperspectral satellites developed by Orbita, are operating in orbit. There is limited open-source hyperspectral image data, resulting in only a small number of open-source HSI datasets being available, which is not conducive to Deep Neural Networks(DNNs) HSI classification. To address this problem, we propose a new HSI dataset "OHID", based on orbital hyperspectral data from Orbita, which has been made available. It is hoped that OHID will assist in improving performance in HSI classification. This paper describes the technical characteristics of OHID, compares it with existing datasets, investigates the use of DNNs in classifying such hyperspectral images, and shows that OHID provides challenges that can help advance the development of HSI classification.

Keywords: Hyperspectral Images · Remote Sensing Dataset · Hyperspectral Satellite · Deep Neural Networks · Classification.

1 Introduction

Hyperspectral remote sensing uses many narrow spectral bands, providing a complete image for each band. Compared with traditional remote sensing with only the three RGB bands, this has many advantages:

• Improved ground object classification: The high spectral resolution of HSI makes subtle differences in appearance and boundaries between objects much easier to detect.

• Better chemical composition analysis: It is much easier to identify the specific light emission and absorption characteristics of various materials.

• Differential analysis: Differences between the image in one band and that in another band can be highly significant.

• Quantitative analysis: Working with narrow spectrum bands can reduce noise and help overcome interference.

These advantages make HSI very useful for many applications, including agricultural analysis, weather forecasting, land and ocean resource surveying, and various others.

Classification of the pixels in the HSI is of basic importance. Currently, classification methods can be divided into supervised classification [15,5,36] and unsupervised classification[32,19]. Classification parameters used typically include Correlation Coefficients, Euclidean Distance, and Mixed Distance.

Supervised classification involves using labeled data to train a model, with the model learning the data features associated with each label by adjusting internal weights until the overall error with the training set is minimized. A large volume of calculations is involved in repetitively adjusting these weights to find the combination that makes the overall error a minimum for the chosen model. However, the huge advances in computing power in recent years have made this approach possible and it is widely used for many purposes, including HSI analysis.

Unsupervised classification involves allowing the system to identify subsets of the data that appear to have related characteristics. This approach is not discussed further here.

DNNs have been found to be a useful supervised approach for many challenging tasks, including image parsing[20,14,11,10,41] and natural language processing [34,43]. Setting up a DNN relies heavily on the availability of appropriately labelled datasets and in recent years these have been published for various tasks [35,25,9,6,12,13]. Examples include CIFAR-10/100 and ImageNet[35] for image recognition, Microsoft COCO[25] and PASCAL VOC[9] for object detection, and ActivityNet[6] and the 'something something' video datasets[12] for video parsing. These datasets are large-scale and well-annotated.

Several datasets have also been published in relation to remote sensing images [8,31]. These can be divided into multiple categories, including standard red-green-blue (RGB) images and HSI. Exploiting HSI[7,37,38,33,40,23,4] is popular since HSI contains rich spectral information that can better present the spatial features and material composition of ground objects. For example, HSI has been used in combination with DNNs to get better precision for object recognition by using information from specific spectrum bands[38] and for the analysis of winter wheat[33].

Available open-source HSI datasets are limited. They include the Indian Pines[1], Salinas Valley[3], and Pavia University[2] datasets. However, on analysis, we find that these older datasets contain a relatively small amount of data and are typically used with traditional algorithms or with shallow DNNs. As shallow DNNs have limited learning capabilities, these networks have limited generalization performance and are not suitable for many practical purposes.

The open-source OHID dataset is intended to help address these limitations. It provides 10 hyperspectral images each with 32 spectral bands ranging from 400nm to 1000nm with image size 512 × 512 pixels, and 7 types of object labels. Its spatial resolution is 10m/pixel. This makes OHID suitable for (i) training DNNs for use with hyperspectral images, (ii) deepening the depth of DNNs, and (iii) improving the generalization performance of DNNs.

Figure 1 shows some sample scenes, with the different parts of the image annotated as described below to indicate the classification of the objects involved. Figure 2 shows a similarly annotated image for part of Zhuhai.

2 Related Works

Three popular aerially photographed HSI datasets are used in many research projects are Indian Pines(IP)[1], Salinas Valley(SV)[3] and Pavia University(PU)[2]. Details of these data and comparisons with OHID are demonstrated in Table 1.

Table 1. Parameters of HSI Datasets.

	IP[1]	SV[3]	PU[2]	OHID
Classes	16	16	9	7
Scenes	1	1	1	**10**
Resolution	20.0m/pixel	3.7m/pixel	1.3m/pixel	10.0m/pixel
Size	145 × 145	512 × 217	610 × 340	512 × 512
Bands	220	224	103	32(240)

OHID is a dataset captured from the hyperspectral satellites of "Zhuhai No. 1" constellation launched by Orbita. It contains 10 scenes and 7 categories of objects. It owns 32 spectral bands selected from 240 spectral bands ranging from 400nm to 1000nm with spectral resolution of 2.5nm and image size 512 × 512 pixels. Its spatial resolution is 10m/pixel.

3 Data Collection and Dataset Design

3.1 Data Collection and Pre-processing

The 'Zhuhai No.1' constellation, which contains 8 hyperspectral satellites[30], was used to collect the OHID dataset. The image processing payload of the satellite has four principal components: (i) the lens, (ii) the focal plane, (iii) the focusing mechanism, (iv) the hood.

After image data was collected, ENVI software was used to perform radiometric calibration, atmospheric correction, and geometric correction on the collected data.

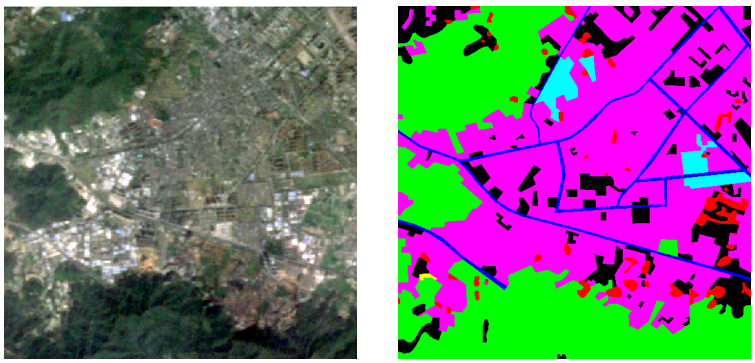

(a) City (b) Annotation of City

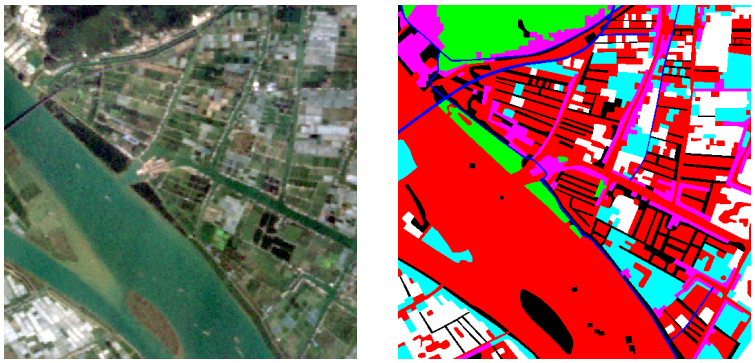

(c) Country (d) Annotation of Country

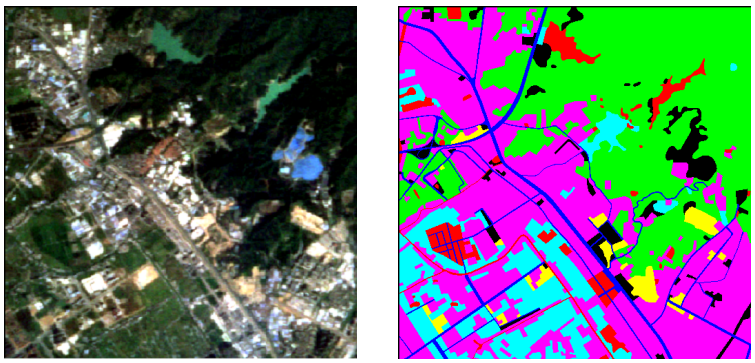

(e) Mountain (f) Annotation of Mountain

Fig. 1. Visualization of OHID. To visualize OHID, we select band 14, 7, 3 as R,G,B, respectively. (a) Visualization of city. (b) Annotation of city. (c) Visualization of country. (d) Annotation of country. (e) Visualization of mountain. (f) Annotation of mountain.

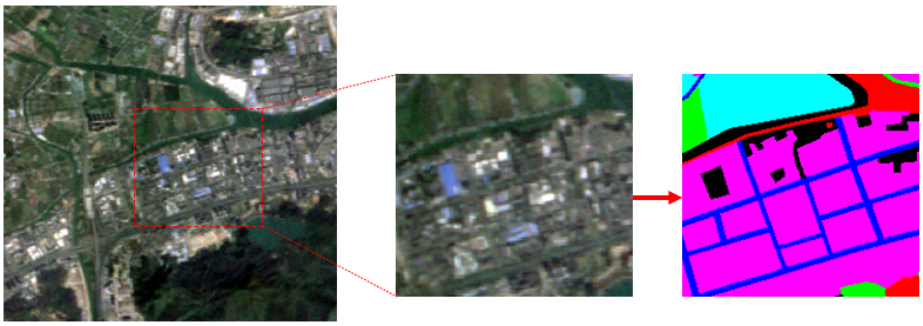

Fig. 2. Annotated OHID image of part of Zhuhai.

First, radiation calibration was calculated with the formula (1):

$$L = gain \times \frac{DN}{TDIStage} + offset \tag{1}$$

where L denotes the apparent radiance, DN denotes the pixel value, $gain$ denotes the absolute radiation calibration gain coefficient, $offset$ denotes the absolute radiation calibration offset coefficient, and $TDIStage$ can be obtained in the field in the image meta data.

Then the FLAASH algorithm was used for atmospheric correction. Based on the location of the study area and the time of image acquisition, we selected the tropical atmospheric correction algorithm, set the aerosol level to urban, and converted the image from apparent radiance data to surface reflectance.

Finally the orthorectification file in the data was used to perform the geometric correction.

Table 2 lists some of these applications and the corresponding spectral bands used. These bands were also used in constructing the OHID dataset.

3.2 OHID Dataset Design

The OHID dataset uses 7 labels, mainly corresponding to basic objects such as buildings and roads, as described in Table 3 below. There are 10 scenes, all of Zhuhai (L: 22.27, E: 113.57), a coastal city in China. All the scenes have the same spatial resolution of 10m/pixel, with 512×512 pixels per scene.

OHID is compressed into a .zip file with size 105MB containing 2 folders, for images and labels respectively:

•images: 10 scenes and 32-band hyperspectral images, .tif format;

•labels: The semantic labels corresponding to the 10 scenes of hyperspectral images, which are single-channel data, again .tif format.

The 10 scenes selected from the collected data for inclusion in OHID were chosen to have a relatively balanced category distribution for the pixels involved, as is seen in Table 3.

Table 2. Parts of Applications of "Zhuhai No.1" Hyperspectral Satellite.

Application	Criteria	Wave Length (nm)	OHID Reference Band
Black and Smelly Water	Chlorophyll Inversion	566 and 670	b7,b14
	Suspended Matter and Transparency	670 and 806	b14,b23
	Black and Smelly Water	550-580 and 626-700	b6-b8 and b11-b17
Water	NDWI	Near red, green light band	b21-b32 and b3-b7
	Suspended Matter Concentration	700-850	b16-b26
	Yellow Substance	466	b1
	Chlorophyll	480,536,566	b2,b5,b7
	Sediment, CODmn	500	b3
	Chlorophyll Absorption	656	b13
	Chlorophyll Fluorescence	686	b15
	Water Plants, Transparency	716	b17
Forestry	Chlorophyll	640-660 and 430-450	b12-b13
	Anthocyanin	537	b5
	FHI (Forest Health Evaluation)	566,606,654,866	b7,b10,b13,b27
	PRI (Photochemical Vegetation Index)	531,570	b5,b7
Crop	RVI (Ratio Vegetation Index), Rice Growth	465-605 and 860-1000	b1-b9 and b27-b32
	SAVI, Wheat Growth	695-750 and 735-1000	b16-b19 and b18-b32
	RVI, Wheat Growth	460-590 and 725-1000	b1-b9 and b18-b32
Ocean	Bleached Coral	520-580	b4-b8
	Water and Land Segmentation	776-940	b21-b32

Table 3. Statistics of Annotation in OHID.

Class	Sample Number	Label
Building	661, 721	1
Farmland	438, 849	2
Forest	370, 901	3
Road	129, 648	4
Water	598, 694	5
Bareland	14, 699	6
Fish Shed	43, 846	7

In order to assure the accuracy of the labeling, we obtained high-resolution aerial flight images with similar dates as a reference and conducted on-site investigations with the help of GPS positioning. For buildings, roads, rivers, large areas of woodland, and other easily distinguishable features, we confirmed and manually outlined these by referring to aerial images, while for bare soil, fish shed, and other features that change rapidly over time we used drones to conduct on-the-spot investigations and used the drone's GPS to match the OHID plot coordinates to obtain accurate features for the image area. Figure 3 is an example of a reference aerial image for each of the 7 categories giving also the corresponding colours used in annotating images.

Fig. 3. Reference aerial images and colours used for annotation.

We also analyzed the reflectance of the scenes at different wavelengths, and Figure 4 presents the average reflectance for each wavelength band for each object class. From this figure it can be seen that the "Zhuhai No.1" satellite performs well in providing the spectral characteristics of each object class and that it shows their difference well. Buildings and roads however are similar in reflectance.

4 Evaluation Metrics and Experimental Results

We analyzed OHID using three HSI classification DNNs to provide a baseline. In what follows we first briefly introduce these three DNNs, then train them with OHID and take experimental results, and finally, we analyze these results and the performance of OHID.

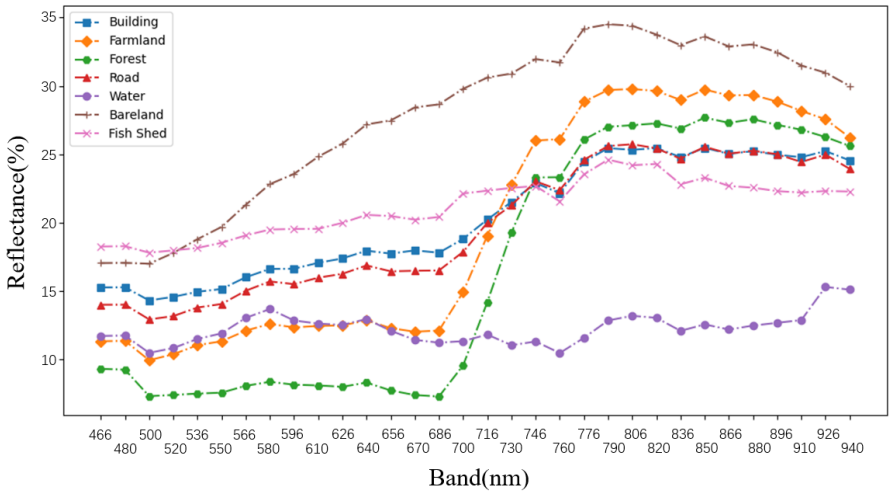

Fig. 4. Reflectance of each object.

4.1 Algorithms Adopted

Tons of methods have been published for optimizing the performance of DNNs in recent years[21,20,14,17,27,26,47,42,46].

For HSI classification, the most successful recent methods include DBDA[24], FDSSC[44], DBMA[29], CDCNN[22], SSRN[45] and DBDA[24].

CDCNN[22] uses a neural network that is deeper than most others. It fuses the ideas of AlexNet[21], DCNN[16], ResNet[14] and FCN[28], and utilizes a residual structure with only convolutional layers used to extract HSI features. However, CDCNN[22] only deals with 2-D data. To address this problem, SSRN[45] adopts 3-D data as input, and improves its structure with ideas from 3DCNN[18] and ResNet[14]. To further improve accuracy, DBMA[29] and DBDA[24] use a novel structure with a dual network to extract features from the space and spectrum of the data separately and merge the features during inference. In other aspects, FDSSC[44] proposes a novel network to improve speed and accuracy.

We adopt CDCNN[22], DBMA[29] and DBDA[24] as the baseline DNNs for our experiment.

4.2 Evaluation Metrics

We utilized the Overall Accuracy(OA), Average Accuracy(AA), and the kappa[39] coefficient to verify HSI classification.

4.3 Experimental Results

We conducted experiments on OHID with three DNNs and a traditional method: (1)CDCNN[22], (2)DBMA[29], (3)DBDA[24], and (4)SVM[15]. We randomly selected 500 samples from each class for training and other samples for testing.

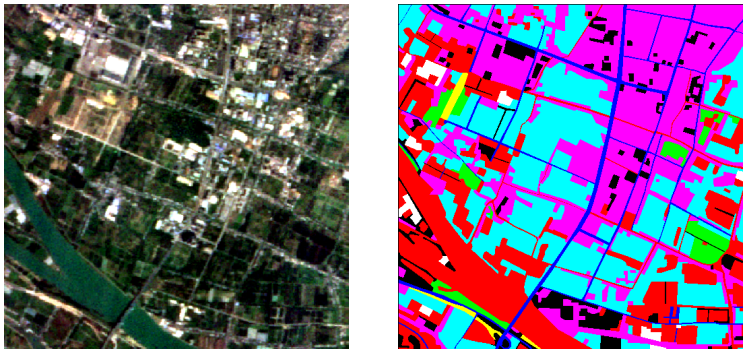

(a) Original Image

(b) Ground Truth Image

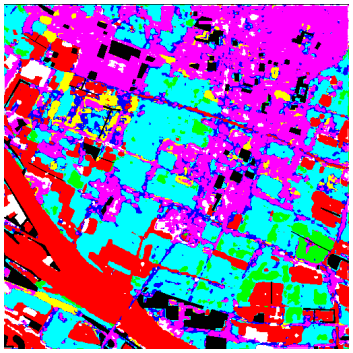

(c) CDCNN[22]

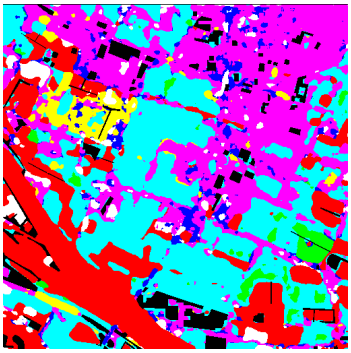

(d) DBMA[29]

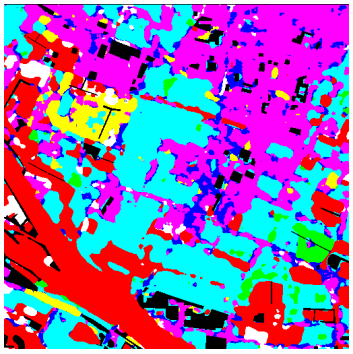

(e) DBDA[24]

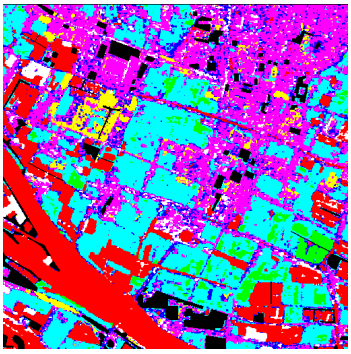

(f) SVM[15]

Fig. 5. Visualization of experimental results. (a)Original images with band 14,7,3. (b)Ground truth annotated image. (c)∼(f) Results.

Table 4. Main Parameters for Training DNNs.

Parameters	Value
Max Epochs	200
Early Stop	30
Learning Rate	0.0001
Batch Size	64

Table 5. Experiment Results on OHID and Other HSI Datasets.

Datasets	Evaluation Metrics(%)	CDCNN[22]	DBMA[29]	DBDA[24]	SVM[15]
IP[1]	OA	62.3	93.2	**95.4**	69.4
	AA	50.9	87.7	**96.5**	65.6
	kappa	55.9	92.2	**94.7**	64.7
PU[2]	OA	87.7	94.7	**96.0**	84.3
	AA	82.4	95.5	**96.5**	83.0
	kappa	83.6	93.0	**94.7**	78.8
SV[3]	OA	77.8	95.4	**97.5**	88.1
	AA	79.9	96.3	**98.0**	91.5
	kappa	75.5	94.9	**97.2**	86.7
OHID	OA	72.4	73.6	**74.0**	69.1
	AA	56.2	60.1	**61.0**	54.3
	kappa	65.3	67.0	**67.5**	61.4

We normalized the data and used the Adam Optimizer and the CrossEntropy Loss for training. We set the learning rate to 0.0001, batch size to 64 by experience and train 200 epochs at a time. The learning rate is reduced by a factor of 0.1 at 50, 90, 110 epoch, respectively. We trained and tested for 10 times and calculated the mean value of OA, AA and the kappa coefficient as our final results. The main parameters are set by experience and they are shown in Table 4. While training SVM[15], we exploited grid search to find parameters *cost* and *gamma*, we set parameter *cost* to 9.514 and parameter *gamma* to 0.03125 and also carried out training and testing 10 times.

The overall experiment results are described in Table 5. We presents several visual results in Figure 5. From the results in Table 5 we can learn that the DNNs gave better performance than SVM, and also that the performance of the chosen DNNs on OHID drops compared to their performance on other datasets, which means that OHID is more difficult for these recent DNNs to annotate correctly. In other words, OHID can provide a good base for the further advancement of HSI classification.

5 Conclusion

This paper describes a new open-source HSI dataset 'OHID' that contains more data than other open-source HSI datasets. We compared OHID with other HSI datasets and also used three well known DNNs to provide a baseline estimate of the difficulty involved in classifying the richer data set provided by OHID. The results show that OHID provides challenges greater than those associated with the previously available HSI datasets. We believe that OHID can contribute to research into HSI and help advance the performance of HSI classification.

For future work, we will expand the capacity of the OHID dataset from 100 MB level to 10 GB level. Meanwhile, we will provide more category labels from 7 classes to over 10 classes, including desert, glacier, wetland, and other terrains. And we will provide data for more regions except for Zhuhai. In addition, we will develop more efficient and accurate classification and detection algorithms as benchmark algorithms based on the characteristics of the OHID to fulfill increasingly diverse application requirements.

6 Acknowledgement

This work is funded by Zhuhai Orbita Aerospace Science & Technology Co. Ltd, China and 2019 Zhuhai Innovation & Entrepreneurship Team Introduction Program under Grant ZH0405-1900-01PWC.

References

1. Indian pines `https://engineering.purdue.edu/~biehl/MultiSpec/hyperspectral.html`
2. Pavia university `http://tlclab.unipv.it/`
3. Salinas valley `http://www.ehu.eus/ccwintco/index.php?title=Hyperspectral_Remote_Sensing_Scenes`
4. Bock, C., Poole, G., Parker, P., Gottwald, T.: Plant disease severity estimated visually, by digital photography and image analysis, and by hyperspectral imaging. Critical reviews in plant sciences **29**(2), 59–107 (2010)
5. Breiman, L.: Random forests. Machine learning **45**(1), 5–32 (2001)
6. Caba Heilbron, F., Escorcia, V., Ghanem, B., Carlos Niebles, J.: activitynet: A large-scale video benchmark for human activity understanding pp. 961–970 (2015)
7. Chen, Y., Zhu, L., Ghamisi, P., Jia, X., Li, G., Tang, L.: Hyperspectral images classification with gabor filtering and convolutional neural network. IEEE Geoscience and Remote Sensing Letters **14**(12), 2355–2359 (2017)
8. Daudt, R.C., Le Saux, B., Boulch, A., Gousseau, Y.: Urban change detection for multispectral earth observation using convolutional neural networks. In: IGARSS 2018-2018 IEEE International Geoscience and Remote Sensing Symposium. pp. 2115–2118. IEEE (2018)
9. Everingham, M., Van Gool, L., Williams, C.K., Winn, J., Zisserman, A.: The pascal visual object classes (voc) challenge. International journal of computer vision **88**(2), 303–338 (2010)

10. Gorbachev, S., Syryamkin, V.: High-performance adaptive neurofuzzy classifier with a parametric tuning. MATEC Web of Conferences **155**, 01037 (2018)
11. Gorbachev, S.V.: Model of intellectual analysis of multidimensional semi-structured data based on deep neuro-fuzzy networks. Machine Learning for Big Data Analysis **1**, 107–148 (2019)
12. Goyal, R., Ebrahimi Kahou, S., Michalski, V., Materzynska, J., Westphal, S., Kim, H., Haenel, V., Fruend, I., Yianilos, P., Mueller-Freitag, M., et al.: The" something something" video database for learning and evaluating visual common sense pp. 5842–5850 (2017)
13. Gu, C., Sun, C., Ross, D.A., Vondrick, C., Pantofaru, C., Li, Y., Vijayanarasimhan, S., Toderici, G., Ricco, S., Sukthankar, R., et al.: Ava: A video dataset of spatio-temporally localized atomic visual actions pp. 6047–6056 (2018)
14. He, K., Zhang, X., Ren, S., Sun, J.: Deep residual learning for image recognition pp. 770–778 (2016)
15. Hearst, M., Dumais, S., Osuna, E., Platt, J., Scholkopf, B.: Support vector machines. IEEE Intelligent Systems and their Applications **13**(4), 18–28 (1998)
16. Hu, W., Huang, Y., Wei, L., Zhang, F., Li, H.: Deep convolutional neural networks for hyperspectral image classification. Journal of Sensors **2015** (2015)
17. Huang, G., Liu, Z., Van Der Maaten, L., Weinberger, K.Q.: Densely connected convolutional networks pp. 4700–4708 (2017)
18. Ji, S., Xu, W., Yang, M., Yu, K.: 3d convolutional neural networks for human action recognition. IEEE transactions on pattern analysis and machine intelligence **35**(1), 221–231 (2012)
19. Ji, X., Henriques, J.F., Vedaldi, A.: Invariant information clustering for unsupervised image classification and segmentation pp. 9865–9874 (2019)
20. Karen, S., Andrew, Z.: Very deep convolutional networks for large-scale image recognition. 3rd International Conference on Learning Representations, ICLR 2015 - Conference Track Proceedings pp. 1–14 (2015)
21. Krizhevsky, A., Sutskever, I., Hinton, G.E.: Imagenet classification with deep convolutional neural networks. Advances in neural information processing systems **25**, 1097–1105 (2012)
22. Lee, H., Kwon, H.: Going deeper with contextual cnn for hyperspectral image classification. IEEE Transactions on Image Processing **26**(10), 4843–4855 (2017)
23. Li, F., Miao, Y., Hennig, S.D., Gnyp, M.L., Chen, X., Jia, L., Bareth, G.: Evaluating hyperspectral vegetation indices for estimating nitrogen concentration of winter wheat at different growth stages. Precision Agriculture **11**(4), 335–357 (2010)
24. Li, R., Zheng, S., Duan, C., Yang, Y., Wang, X.: Classification of hyperspectral image based on double-branch dual-attention mechanism network. Remote Sensing **12**(3), 582 (2020)
25. Lin, T.Y., Maire, M., Belongie, S., Hays, J., Perona, P., Ramanan, D., Dollár, P., Zitnick, C.L.: Microsoft coco: Common objects in context pp. 740–755 (2014)
26. Liu, W., Zhang, Y., Yan, J., Zou, Y., Cui, Z.: The Semantic Segmentation Network for Remote Sensing Image with Dynamic Perceptual Loss. IEEE Access pp. 1–17 (2020)
27. Liu, W., Zhang, Y., Yan, J., Zou, Y., Cui, Z.: Semantic Segmentation Network of Remote Sensing Images with Dynamic Loss Fusion Strategy. IEEE Access **9**, 70406–70418 (2021)
28. Long, J., Shelhamer, E., Darrell, T.: Fully convolutional networks for semantic segmentation pp. 3431–3440 (2015)

29. Ma, W., Yang, Q., Wu, Y., Zhao, W., Zhang, X.: Double-branch multi-attention mechanism network for hyperspectral image classification. Remote Sensing **11**(11), 1307 (2019)
30. Meng, J., Wu, J., Lu, L., Li, Q., Zhang, Q., Feng, S., Yan, J.: A Full-Spectrum Registration Method for Zhuhai-1 Satellite Hyperspectral Imagery. Sensors **20**(21), 6298 (2020)
31. Mohanty, S.P.: Crowdai dataset (2018), `https://www.crowdai.org/challenges/mapping-challenge/dataset_files`
32. Park, S., Han, S., Kim, S., Kim, D., Park, S., Hong, S., Cha, M.: Improving Unsupervised Image Clustering With Robust Learning. CVPR (2), 12278–12287 (2021)
33. Prey, L., Von Bloh, M., Schmidhalter, U.: Evaluating rgb imaging and multispectral active and hyperspectral passive sensing for assessing early plant vigor in winter wheat. Sensors **18**(9), 2931 (2018)
34. Rafal, J., Wojciech, Z., Ilya, S.: An empirical exploration of Recurrent Network architectures. 32nd International Conference on Machine Learning, ICML **3**, 2332–2340 (2015)
35. Russakovsky, O., Deng, J., Su, H., Krause, J., Satheesh, S., Ma, S., Huang, Z., Karpathy, A., Khosla, A., Bernstein, M., Berg, A.C., Fei-Fei, L.: ImageNet Large Scale Visual Recognition Challenge. International Journal of Computer Vision **115**(3), 211–252 (2015)
36. Sammut, C., Webb, G.I.: Naive bayes pp. 713–714 (2010)
37. Sellami, A., Abbes, A.B., Barra, V., Farah, I.R.: Fused 3-d spectral-spatial deep neural networks and spectral clustering for hyperspectral image classification. Pattern Recognition Letters **138**, 594–600 (2020)
38. Sellami, A., Tabbone, S.: Deep neural networks-based relevant latent representation learning for hyperspectral image classification. Pattern Recognition **121**, 108224 (2022)
39. Sim, J., Wright, C.C.: The kappa statistic in reliability studies: use, interpretation, and sample size requirements. Physical therapy **85**(3), 257–268 (2005)
40. Swatantran, A., Dubayah, R., Roberts, D., Hofton, M., Blair, J.B.: Mapping biomass and stress in the sierra nevada using lidar and hyperspectral data fusion. Remote Sensing of Environment **115**(11), 2917–2930 (2011)
41. Syryamkin, V.I., Gorbachev, S.V., Shikhman, M.V.: Adaptive neuro-fuzzy classifier for evaluating the technology effectiveness based on the modified wang and mendel fuzzy neural production mimo-network. IOP Conference Series: Materials Science and Engineering **516(1)**, 012037 (2019)
42. Tan, S., Yan, J., Jiang, Z., Huang, L.: Approach for improving YOLOv5 network with application to remote sensing target detection. Journal of Applied Remote Sensing **15**(03), 036512 (2021)
43. Vaswani, A., Shazeer, N., Parmar, N., Uszkoreit, J., Jones, L., Gomez, A.N., Kaiser, Ł., Polosukhin, I.: Attention is all you need pp. 5998–6008 (2017)
44. Wang, W., Dou, S., Jiang, Z., Sun, L.: A fast dense spectral–spatial convolution network framework for hyperspectral images classification. Remote Sensing **10**(7), 1068 (2018)
45. Zhong, Z., Li, J., Luo, Z., Chapman, M.: Spectral–spatial residual network for hyperspectral image classification: A 3-d deep learning framework. IEEE Transactions on Geoscience and Remote Sensing **56**(2), 847–858 (2017)
46. Zou, Y., Zhang, Y., Yan, J., Jiang, X., Huang, T., Fan, H., Cui, Z.: A Robust License Plate Recognition Model Based on Bi-LSTM. IEEE Access **8**, 211630–211641 (2020)

47. Zou, Y., Zhang, Y., Yan, J., Jiang, X., Huang, T., Fan, H., Cui, Z.: License plate detection and recognition based on YOLOv3 and ILPRNET. Signal, Image and Video Processing (2021)